CI&CEQ
Chemical Industry & Chemical Engineering Quarterly

Available online at
Association of the Chemical Engineers of Serbia AChE
www.ache.org.rs/CICEQ

Chem. Ind. Chem. Eng. Q. 30 (3) 193–206 (2024) CI&CEQ

HEITOR OTACÍLIO NOGUEIRA ALTINO[1]
GIOVANI AUD LOURENÇO[2]
CARLOS HENRIQUE ATAÍDE[1]
CLAUDIO ROBERTO DUARTE[1]

[1]Federal University of Uberlandia, Faculty of Chemical Engineering, Uberlândia, MG, Brazil

[2]Federal Institute of Goiás, Itumbiara, GO, Brazil

SCIENTIFIC PAPER

UDC 621.3.04:621.317:66

THE INFLUENCE OF MOISTURE CONTENT ON DRILLED CUTTINGS' PROPERTIES OF BED PACKING AND FLOWABILITY

Article Highlights

- Extensive analysis of moisture on drilling cuttings' bed packing and flowability
- Four characteristic states are identified according to the moisture level of cuttings
- The interparticle structures become looser and steadier as moisture rises to 15.2%
- Beyond 15.2%, moisture increases provide denser and less stable structures
- Predictive models proposed for moisture's influence on bed packing and flowability

Abstract

To design and operate various equipment of the solids control system in offshore drilling platforms, it is important to establish how the moisture content influences the characteristics of drilled cuttings to form packed beds and flow over solid surfaces. The current study comprehensively analyzes how moisture content, primarily composed of water and representing water-based muds (WBMs), influences the bed packing properties and drilled cuttings' flowability. The particle aggregation/disaggregation dynamics, loose and tapped bulk densities and porosities, compaction dynamics of packed beds, Hausner ratio, and angle of repose of drilled cuttings with ten distinct moisture contents (1.4–44.0 wt%) were analyzed. It was noticed that the increment of moisture content up to 15.2% promoted the formation of looser interparticle structures. However, these structures were steadier, showing greater difficulty flowing and releasing air/liquid. The continuous increment of moisture content beyond 15.2% promoted a complete change in the material behavior. The interparticle structures became denser. The material could flow and release air/liquid more easily. In addition, it was possible to establish a classification of the different behaviors of drilled cuttings according to the moisture content. Predictive models were proposed to describe the influence of the moisture content on the bed packing and flowability properties of drilled cuttings.

Keywords: particle aggregation, particle disaggregation, packed bed, flowability, compaction.

Oil and gas production is an important part of meeting global energy demand, with total production forecast to grow by 17 million barrels of oil equivalent per day by 2025. The expectations are that offshore production will be responsible for approximately 5 million barrels of oil equivalent in 2025, representing 29% of the total oil and gas production [1]. The offshore wells are drilled using a rotating drill bit connected to a drilling platform through a hollow pipe, which is rotated using an electric or hydraulic motor to obtain oil and gas. To maintain the pressure, lubricate, and reduce the temperature of the drill bit, a drilling fluid is injected inside the hollow pipe and returned to the platform through the annulus between the drill string and the wall of the drilled hole. In general, drilling fluids are classified according to their main constituents, such as Water-based muds (WBMs), Oil-based muds (OBMs),

Correspondence: C.R. Duarte, Federal University of Uberlandia, Faculty of Chemical Engineering, Av. João Naves de Ávila, 2121, Block 1K, 38408-100 Uberlândia, MG, Brazil.
E-mail: claudioduarte@ufu.br
Paper received: 24 April, 2023
Paper revised: 11 August, 2023
Paper accepted: 28 August, 2023

https://doi.org/10.2298/CICEQ230424023A

and Synthetic-based muds (SBMs). Due to environmental and cost concerns, WBMs have become the preferred choice in this category [2,3]. As the drill bit rotates and grinds the rock formations, small rock particles, known as drilled cuttings, are generated and suspended in the drilling fluid, returning to the platform along with the fluid. The cuttings are separated by a set of unit operations in a solid control system in the platform, and the drilling fluid returns to the drilling process. Depending on the local legislation, the separated cuttings can be disposed of in different ways: re-injection into offshore wells, onshore treatment and disposal, and discharge into marine environments after adequate treatment. To dispose of the drilled cuttings must be conveyed from the drilling platform to the conveying vessels. For this purpose, several methods can be utilized, such as skip-and-ship, conveyor belts, screw conveyors, and pneumatic conveying [4].

One of the main challenges of handling drilled cuttings is that the material is very naturally inconsistent [5]. In particular, drilled cuttings' moisture content (MC) is a critical variable, consisting of a mixture of water and oil. In the case of drilled cuttings containing WBMs, the MC primarily comprises water, as a significant portion of this drilling fluid comprises it [4]. It is possible to observe drilled cuttings in the form of pastes, with more than 60% by weight of MC, and in the form of granular solids, with less than 5%. Such moisture contents depend on several factors, such as drilling rates and conditions, drilling fluids used, solids control equipment efficiency, and from what stage of the solids control system the cuttings originate [4,5]. Nevertheless, this last factor is one of the most important, e.g., some patents describe that the drilled cuttings coming from shale shakers may be free-flowing, non-free-flowing, or pasty, with moistures ranging from 10 to 20% by weight. On the other hand, drilled cuttings from the bottom of Vortex dryers are generally solids with good flowability, with 5% moisture. While drilled cuttings coming from the cuttings processor may be free-flowing or non-free-flowing, depending on how much fluid the equipment removes [6–11].

In the unit operations of the solids control system and the conveying stage to the vessel, the material is stored in silos, tanks, and blow tanks and flows through gutters, discharge valves, and conveying pipes [6–11]. However, due to the significant changes in the moisture content of the material during these processes, the bed packing and flowability properties are completely altered, leading to changes in the bulk behavior of the material. Thus, it is important to know how the MC can affect these properties to design systems to convey, store, and discharge drilled cuttings. Bed packing properties, e.g., are needed to determine the bulk volume of material that can be packed into a blow tank or microwave treatment equipment and the volume changes that can be expected due to systems vibrations [12–15]. The flowability properties describe the relative movement of a bulk of particles among neighboring particles or along solid surfaces, e.g., gutters and pipes [16]. Furthermore, it's important to highlight that during the operation of drilled cuttings handling systems, the lack of knowledge of how *MC* affects these properties can lead to low process efficiencies and clogging problems. In more extreme cases, these clogging problems can stop the entire drilling process once the drilled cuttings cannot be disposed of [4,5,8].

Generally, such properties are governed by complex interactions between internal and external forces. A cohesive behavior is expected if the external forces are lower than the interparticle forces [17]. Friction and cohesion are the major interparticle forces acting on the material. Friction acts at the contact points of the particles, opposing the relative motion between them. In this case, the shape and surface morphology of the particles directly affects the friction forces. Cohesion refers to the forces of attraction between particles, including van der Waals forces, local chemical bonds, electrostatic charges, and liquid bridging forces, originating from net surface tension [17,18]. In the case of sand-like non-porous materials, such as drilled cuttings, moisture is preferentially adhered to the surface of the particles, influencing both frictional and cohesion forces [12,17]. At first, the cohesion forces are the most affected by the increase in moisture due to the strengthening of the liquid bridge bonds between the particles, which reduces the particles' easy movement [17,18]. However, as reported by several authors [18,19], at a certain amount, moisture can also simultaneously act as a lubricant for the particles, reducing frictional forces and increasing the facility for the particles to move.

Several parameters can be used to measure how the properties of bed packing and flowability can be affected by the MC. The loose and tapped bulk densities and porosities indicate how the moisture content can influence the relative rearrangement of particles to form packed beds. The flowability of materials can be indirectly estimated and classified by the Hausner ratio and the angle of repose. In addition, these indicators also provide important information on the inter-particular forces present in the material [16]. It is also highlighted that changes in interparticle forces can induce particles to aggregate into clusters or disaggregate, making it possible to quantify these phenomena by analyzing the particle size distribution of the material [20].

However, studies addressing the influence of *MC* on the packing and flowability characteristics of drilled cuttings are still scarce in the literature. In large part, there is only the description of the material's behavior according to moisture performed by some patents, as previously mentioned [6–11]. Nevertheless, the moisture content ranges at which the material bulk behavior changes and the interparticle forces involved were still not studied. Some authors also report that the flowability of drilled cuttings can be improved by adding the correct amount of dilution fluid, such as water [5]. However, it is not known the saturation point at which it occurs.

Furthermore, even analyzing papers [21,22] that described the effect of moisture content on the bed packing properties of materials similar to drilled cuttings, such as sands, it is possible to observe that low moisture content ranges are generally analyzed, not contemplating the entire range described in patents [6–11].

Among the works consulted, no information was found on the loose and tapped bulk densities and porosities, as well as the Hausner ratio and angle of repose of drilled cuttings with different moisture contents. Thus, a comparative analysis of how the moisture content influences the packing properties and flowability of cuttings and the dynamics of aggregation/disaggregation of the particles is necessary. This analysis may help to elucidate the different effects of moisture on cutting management characteristics reported in the patents [6–11]. Consequently, from a practical point of view, this analysis can improve drilled cuttings management operations.

In this context, this study aimed to analyze how moisture content, primarily consisting of water and representing WBMs, affects the properties of bed packing and flowability of drilled cuttings. For this purpose, the influence of ten distinct moisture contents of drilled cuttings was studied on the particle size distribution, loose and tapped bulk densities and porosities, compaction dynamics of packed beds, Hausner ratio, and angle of repose. The analysis of these parameters allowed the establishment of a classification of the different behaviors of drilled cuttings according to the moisture content, reinforcing this paper's novelty. The main interparticle forces involved and the general handling behavior of the material in each state of the classification were discussed.

Furthermore, predictive models were proposed to describe the influence of the moisture content of drilled cuttings on the studied parameters.

MATERIALS AND METHODS

Drilled cuttings

The drilled cuttings were provided by Petróleo Brasileiro S.A. (Petrobras®). The material was sampled after the processing stage through the shale shakers and originates from the drilling of carbonate rocks in the depth range of 4656 to 4758 meters in Campos Basin, Campos, Rio de Janeiro, Brazil. The drilling process used a polymeric water-based drilling fluid with xanthan gum and modified starch. Table S1 and Figure S1 (Supplementary Material) show details of the characteristics of the dry material.

Oil, water, and solids contents

The contents of oil, water, and solids of the drilled cuttings were determined by the retort test in duplicates, using the gravimetric method, according to API [23], allowing to determine the contents of oil (C_o), water (C_w), and solids (C_s).

Characterization of dry drilled cuttings

The apparent density (ρ_a) was estimated using the technique of liquid pycnometry with pure deionized water at 25.0°C. The actual density (ρ_r) of the drilled cuttings was determined in triplicate utilizing a gas pycnometer (He) (Micromeritics®, Accupyc 1330). The establishment of the apparent and actual densities allows the estimation of the particle porosity (ε_p) by the following equation:

$$\varepsilon_p = 1 - \frac{\rho_a}{\rho_r} \tag{1}$$

The sphericity (φ) of five hundred particles was determined using the image analysis technique. An optical microscope (Nikon®, Eclipse E-200) equipped with a digital camera (Motic®, Moticam 5) was used for capturing the images. The Image-Pro Plus® 6.0 software was used to establish the particles' area (A) and perimeter (P). Sphericity was calculated by the equation:

$$\varphi = \frac{4\pi A}{P^2} \tag{2}$$

The size distribution of the particles was determined in triplicate by the sieving method described by ASTM [24]. To describe the particle size distribution, the Rosin-Rammler-Bennet model (RRB), specified by Eq. (3), was fitted to the experimental data [25].

$$Y(x) = 1 - e^{-\left(\frac{x}{x_0}\right)^n} \tag{3}$$

where $Y(x)$ is the cumulative fraction of material by

weight less than size x, x is the particle size, n is the uniformity constant, and x_0 is the characteristic particle size.

The surface morphology and elements of the particles were analyzed by scanning electron microscopy (SEM) and energy dispersive spectroscopy (EDS). Initially, the samples were overlaid with a thin layer of gold (75 nm) using a Leica® EM SCD050 spray device. Then, the characterization was performed using a Zeiss® EVO MA10 microscope and an Oxford® 51-ADD0048 detector. The magnifications of 300x, 1000x, and 5000x were evaluated.

Material humidification procedure

In this paper, the moisture content (*MC*) is referred to as the sum of the contents of water and oil, as shown by Eq. (4). The saturation level (*S*) can be defined as the fraction of interparticle volume of a packed bed that is filled with a liquid and was calculated by Eq. (5).

$$MC(\%g.g^{-1}) = \frac{m_w + m_o}{m_w + m_o + m_s} 100 \quad (4)$$

$$S(\%mL.mL^{-1}) = \frac{V_{liq}}{V_t - V_s} 100 \quad (5)$$

where m_w is the mass of water, m_o is the mass of oil, m_s is the mass of solid, V_{liq} is the total volume of liquid (water + small amounts of oil in the solid particles) in the bed, V_t is the total volume of the dry bed, and V_s is the volume occupied by the solid (based on actual density). The residual oil in the solid particles was identified by gas chromatography coupled to mass spectrometry (Shimadzu®, GCMS-QP2010) as 1- pentadecene ($C_{15}H_{30}$). The oil density of 0.781 ± 0.001 g/mL was obtained by liquid pycnometry at 20°C. The oil viscosity of 2.4×10^{-3} Pa.s was determined in a rheometer (Brookfield®, R/S plus) at 20°C.

It's important to highlight that, in general, WBMs are mainly composed of water (≈76%) [4]. Therefore, pure water was employed to humidify the cuttings, aiming to simulate the impact of WBMs content on particle aggregation/disaggregation, bed packing, and flowability dynamics. It is also important to highlight that although the dry drilled cuttings had a residual amount of oil (1-pentadecene), the quantity of it was very small (1%<) and reduced even more (0.5%<) when the material was humidified for higher MCs, due to the solid concentration reduction. Therefore, the material was not submitted by any cleaning process of the oil before the humidification process. Thus, the primary effect of moisture on the drilled cuttings properties analyzed was considered to be due to the action of the water.

The material was humidified to reach ten different *MC*s: 1.3%, 5.4%, 7.7%, 10.0%, 12.5%, 15.2%, 21.0%, 27.6%, 35.2% and 44.0%, as seen in Figure 1. The compositions of oil, water, and solids for each MC analyzed can be observed in Table S2. These moisture contents correspond to the saturation levels of 5.4%, 18.9%, 25.7%, 32.5%, 39.2%, 46.0%, 59.5%, 73.0%, 86.5% and 100.0%, which covers the three characteristic wet powder states, described here only as a reference: pendular (0% to 25%), funicular (25% to 80-90%), and capillary (80-90% to 100%) [18,19]. The humidification procedure included adding the necessary material to a zip-lock bag. Then, the deionized water needed to reach the desired *MC* was added. The bag was sealed, and the mixture was manually mixed for over 10 min. The bag remained closed for at least 1 h to complete the homogenization of the mixture. This specific duration was established as the minimum required time to ensure uniform moisture distribution across the entire zip lock bag. After this time, the desired characteristics of the material were analyzed (aggregation/disaggregation dynamic, bed packing, and flowability). It's important to highlight that the humidified material was not reused from one analysis to the other. In each analysis, a new humidification process was performed. The material was submitted to a retort test to check if the desired moisture content was obtained.

Optical microscopy

Optical microscopy was used to observe the effect of the *MC* on the visual aspect of drilled cuttings and to quantify the particle agglomeration/aggregation. An optical microscope (Nikon®, Eclipse E-200) equipped with a digital camera (Motic®, Moticam 5) was used for capturing the images. The mean diameter of more than one hundred particles and particles' clusters was obtained using the Image-Pro Plus® 6.0 software for each *MC* studied. It is important to highlight that the particle diameter alteration analyzed can also be due to water absorption by the drilling cuttings. Nevertheless, due to the low particle porosity of the material (0.0355), this can be considered a minor effect.

Determination of bed packing properties

The loose (ρ_0) and tapped (ρ_t) bulk densities of drilled cuttings were determined in triplicate according to the main norms for bulk density establishment [26,27]. The automated system for bulk density data acquisition of granular materials described by Altino *et al.* [28] was used for this purpose. The number, frequency, and amplitude of the taps were 3000, 250 taps/min, and 16.0 mm. These conditions were observed by Altino *et al.* [28] to promote the optimal

packing of sand "S50". Thus, due to the similarity between drilled cuttings and sands and the strong interparticle cohesion forces induced by moisture, these conditions were chosen to be utilized in this paper. A plastic tube (internal diameter of 21.20 mm, external diameter of 25.00 mm, and height of 275 mm) was concentrically placed on the graduated cylinder to pack the material in the graduated cylinder. The material was introduced into the plastic tube by pouring constant amounts of material from the same height with a funnel. After filling the tube with the material, the tube was removed at a constant speed of 12.2 ± 1.5 mm/s. The powder gradually flowed off the tube and packed into the graduated cylinder. For each *MC* analyzed, the mass of the material was selected to promote the initial packing volume of 100 mL. This packing method ensured precise initial volumes of packed material with low variability.

The loose porosity (ε_0), tapped bulk porosity (ε_t), and effective porosity (ε_{eff}) of the material were respectively determined by Eqs. (6–8) [28,29]. The calculations involving ε_0, ε_t, and ε_{eff} were performed by discounting the mass of liquid (water + small amounts of oil (1-pentadecene) in the solid particles) from the total mass of the packed bed. As porosity describes the bed structure, there is no point in considering the liquid's mass [22].

$$\varepsilon_0 = \frac{V_{intra} + V_t}{V_{bulk}} + \frac{V_{add}}{V_{bulk}} \quad (6)$$

$$\varepsilon_t = \frac{V_{intra} + V_{opt}}{V_{bulk}} \quad (7)$$

$$\varepsilon_{eff} = \frac{V_{intra} + V_t + V_{add} - V_{liq}}{V_{bulk}} \quad (8)$$

where V_{bulk} is the bulk volume, V_{intra} is the intra-particular volume, V_t is the sum of the inter-particular voids when the granular system is in an optimal packaging state, V_{add} is the additional volume trapped in the packaged material, and V_{liq} is the volume of liquid occupying the interparticle voids spaces.

The ability of the material to release trapped air/liquid was evaluated by the additional porosity (ε_{add}), calculated by Eq. (9). While the air/liquid release kinetic due to the compaction of the pecked bed was measured by the granular relaxation index ($\tau_{½}$), according to Eq. (10). This parameter represents the ratio between the packing fraction variation and the number of taps needed to reach the middle of the compaction process ($N_{½}$) [29].

$$\varepsilon_{add} = \frac{\varepsilon_0 - \varepsilon_t}{\varepsilon_0} \quad (9)$$

$$\tau_{1/2} = (D_t - D_0) N_{1/2} \quad (10)$$

where D_t is the packing fraction of the compacted material, and D_0 is the packing fraction of the loose material.

The experiments were performed at room temperature (25.2 ± 0.5°C) with relative air moisture of 55.4 ± 2.7%, sufficient to eliminate the static charges visually.

Determination of flowability indicators

The flowability of the drilling cuttings was analyzed by two indicators: static angle of repose (*AoR*) and the Hausner ratio (*HR*) in triplicates. The first one was determined based on the funnel method described by ASTM [30]. Further details of the experimental system can be found in Altino *et al.* [28]. It is important to highlight that for the material with moisture contents higher than 15.2%, it was impossible to determine the angle of repose due to the slurry behavior of the mixture. The second indicator (*HR*) was calculated by the ratio between the tapped bulk density and the loose bulk density, based on the method described by the WHO [31].

RESULTS AND DISCUSSION

Characterization of dry drilled cuttings

Table S1 shows that the base material had low water and oil contents, being suitable to be humidified. Nevertheless, to understand how moisture can affect the behavior of the drilled cuttings, It is important to classify it as a porous or non-porous material. In general, for porous materials, moisture fills the particle porous and adds weight to the bed, increasing the density of the material. On the other hand, for non-porous materials, surface moisture contributes to liquid bridge forces, altering the interparticle forces (cohesion forces) [22]. According to Ishizaki *et al.* [32], porous materials have particle porosities (ε_p) that range between 0.2 and 0.95. Thus, according to particle porosity obtained by Eq. (1) for the drilled cuttings studied, it can be classified as a non-porous material.

The sphericity (φ) of the drilled cuttings was according to the value reported by Hyun *et al.* [33] (0.80). The apparent (ρ_a) and real (ρ_r) densities of the material also were according to the real density reported by Petri *et al.* [34] (2.6830 g.cm^{-3}). The Sauter mean diameter (D_{Sauter}), on the other hand, was lower than the value reported by Petri *et al.* [34] (238 μm). Based on the values of real density and Sauter mean diameter of Table S1, the drilled cuttings can be classified as Geldart B-type [35].

The SEM micrographs in Figure S1 show particles

without defined pores with various sizes and shapes, rough surfaces, and asperities. The presence of particle agglomerates can also be observed, highlighting the material's cohesiveness. The EDS results (Figure S1d) evidenced the existence of several elements in drilled cuttings particles. Carbon and gold appear in large quantities. However, it's important to highlight that the particles were coated with gold and attached to a conductive carbon adhesive tape (Nisshin®, Nem Tape) to carry out the analyses. It is also possible to observe significant amounts of calcium, oxygen, and magnesium. The drilled cuttings analyzed were sourced from carbonate rocks. According to Reeder [36], those rocks are mainly formed by calcite ($CaCO_3$), dolomite ($CaMg(CO_3)_2$), and aragonite ($CaCO_3$), which may be the source of the observed elements.

Effect of moisture content on drilled cuttings properties

Particle aggregation and disaggregation

The effect of the *MC* on the visual aspect of the drilled cuttings is shown in the micrographs in Figure 1. The small variations between the scales of the figures allowed for performing a comparative analysis of MC's influence on the cuttings' visual aspect. The increase of *MC* up to 15.2% (Figure 1f) promoted a reduction in the number of fine particles and small particles' clusters, while the size of the larger particles' clusters increased. For higher *MC*s, the material started to change to a pasty state, increasing the number of fine particles and small particle clusters and reducing the size of the larger clusters. The increase of particles' clusters and reduction of fines and small particles' clusters with increased *MC* can be either agglomeration or aggregation [37,38]. Nevertheless, as the clustering of the particles showed to be reversible by the increase of *MC*, the phenomena can be classified as aggregation [38].

To quantify the alterations of the particle sizes in the function of the *MC*, the mean particle diameter and the number of fines lower than 75 μm were determined [37]. The results are presented in Figure 2. It is crucial to emphasize that the particle sizes quantification was performed centered around the mean Sauter diameter (161.73 μm, Table S1) once the optical microscopy does not allow the analysis of the whole particle size range of the drilled cuttings (20–3350 μm). However, these results offer valuable insights into how the moisture content affects the aggregation and disaggregation dynamics of the particles with sizes similar to the mean particle size of the material. A scheme, shown in Figure 3, was created to elucidate the phenomena better. The *MC*s' limits, states, and substates illustrated in Figure 3 were established in this paper based on the similar behaviors of the particles considering aggregation, bed packing, and flowability characteristics. These limits are also marked in Figure 2.

In the dry state (1) (Figure 3), the saturation level range is of the pendular state. The particles were dispersed, and the mean particle diameter remained almost constant with the increment of *MC*. It is expected, considering the weak liquid bridge forces generally observed in the pendular state [18]. Proceeding to the aggregated substate (2a) (Figure 3),

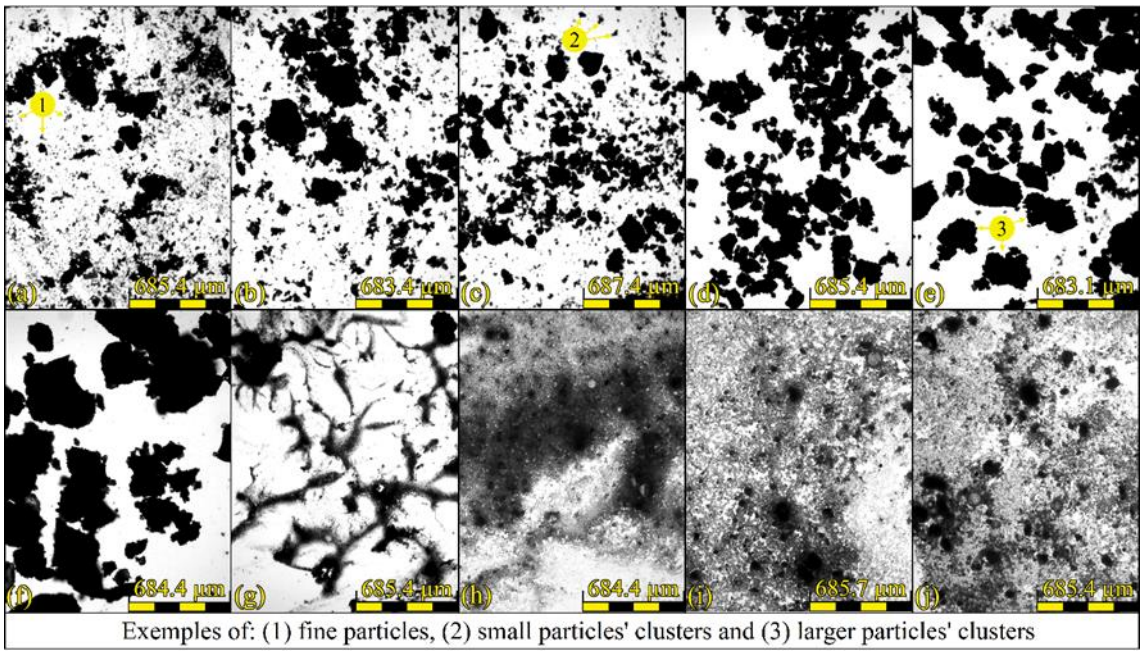

Figure 1. Micrographs of drilled cuttings with different moisture contents: (a) 1.3%; (b) 5.4%; (c) 7.7%; (d) 10.0%; (e) 12.5%; (f) 15.2%; (g) 21.0%; (h) 27.6%; (i) 35.2% and (j) 44.0.

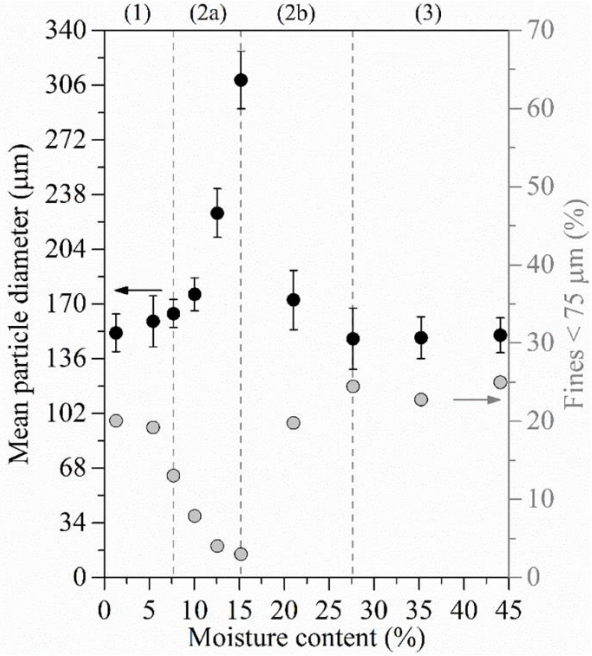

Figure 2. Effect of the moisture content on the mean particle diameter and content of fines of drilled cuttings, assessed using optical microscopy.

as the *MC* increases, the mean diameter increases increases, and the content of fines reduces up to the *MC* of 15.2% (2a). The saturation level range is of the funicular state. Thus, increasing *MC* may induce liquid bridges to form, increasing the interparticle forces and promoting the aggregation of fines and small particles into clusters of larger diameters. After this, on disaggregated substate (2b) (Figure 3), the amount of liquid seems to be just enough to start a gradual dispersion of the aggregates into clusters of smaller diameter and fines. The MC of 15.2% is believed to be sufficient to start the saturation of some interparticle spaces, spacing out particles and reducing the cohesion forces. At the same time, when enough moisture is present on the surface of the particles, it creates a layer of liquid that can act as a lubricating film between the particles, reducing the resistance to particle motion by minimizing the frictional forces at the contact points [17]. Thus, it is hypothesized that the reduction of the cohesion forces on substate (2b) and the lubricating action of the particle's surfaces allowed the dispersion of the aggregates.

Finally, at 27.6%, a saturation point is achieved, initiating the slurry state (3) (Figure 3), where the saturation level is of a capillary state. It's possible to observe that the aggregates were dispersed so that the mean particle diameter and fine amount were similar to those of the dry state (1). It is important to highlight that the aggregation and desegregation of particles are very complex phenomena, and several factors may also contribute to the observed results. For example, the drilled cuttings studied were sourced from carbonate rocks, which are well-known for their very low solubility in water [39]. This characteristic can impact the dynamics of particle aggregation/desegregation and particle sizes. Furthermore, the initial sample may contain clusters that tend to disaggregate under high moisture content. This observation is supported by the slightly higher amount of fines observed in the slurry state (3) (≈ 24%) compared to the dry state (1) (≈20%).

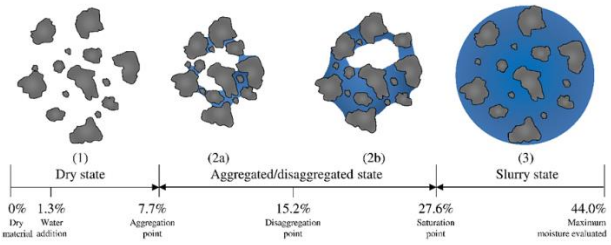

Figure 3. Schematic of the behavior of the particles with increasing moisture content.

Bed packing properties

The compaction curves of drilled cuttings with different *MC*s are shown in Figure S2. To check if the tapping number was enough to achieve the stationary state, the values of ρ_t were compared with values of asymptotic bulk density (ρ_∞). This last parameter was acquired by the fit of the KWW model [40] to the experimental data. The results presented in Table S3 show good adjustments of the model to the data, as demonstrated by high values of coefficients of determination (R^2). A Student's t-test, performed between ρ_t and ρ_∞, showed, with 95% reliability, that there is no statistically significant difference between the data, as evidenced by the *p-values* in this table. Thus, the number of taps provided for obtaining the tapped bulk density was sufficient to reach the stationary state predicted by the model for each *MC* analyzed.

The influence of *MC* on the loose (ρ_0) and tapped (ρ_t) *bulk* densities of drilled cuttings is displayed in Figure S3. The effect of *MC* on the packed bed characteristics can be better interpreted by analyzing the loose (ε_0) and tapped (ε_t) bulk porosities, displayed in Figure 4. The states' limits of Figure 3 were marked for better data analysis. The loose and tapped *bulk* porosities represent the fraction of void volume regarding the total volume of the bed, no matter whether these voids are filled with liquid or air. In states (1) and (2a), it is possible to observe that the loose and tapped bulk porosities increase with the increment of moisture up to 15.2% for ε_0 and 12.5% for ε_t. This behavior can be attributed to increased cohesion forces through strengthening liquid bridges between particles, as illustrated in Figure 3 (2a) [22,41]. Consequently, the particles have more difficulty rearranging their relative positions to form denser pecked beds (lower porosity),

resulting in looser-packed beds [22]. It may be expected that ε_t would also show a turning point at *MC* of 15.2%, as was observed for ε_0. Nevertheless, in the compaction process, energy is applied to the packed bed to cause the rearrangement of the relative positions of the particles. Thus, as the compaction process proceeds, the void spaces are reduced, and the saturation level gradually increases [16]. The saturation level is estimated to increase due to compaction from 46.0% to 53.3% at an *MC* of 15.2%. In this higher saturation level, the cohesion and friction forces are reduced, allowing the particles to rearrange into a denser bed configuration.

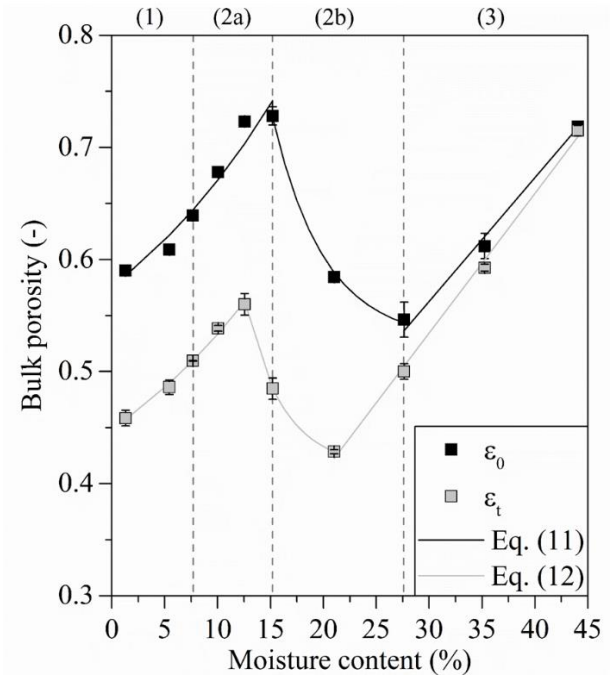

Figure 4. Effect of moisture content on loose (ε_0) and tapped (ε_t) bulk porosities of drilled cuttings.

After this point, on the substate (2b) of Figure 4, the increase of *MC* resulted in a decrease of ε_0 and ε_t, probably due to the reduced cohesion forces previously mentioned [22,41]. This reduction goes up at 27.6% for ε_0 and 21.0% for ε_t. It is interesting to highlight that, at these points, the porosities observed were similar to those of the dry material (1.3%). Once again, it may be expected that ε_t would present a turning point at 27.6%, as perceived for ε_0. However, as cited before, the compaction process increases the saturation level. In this case, the saturation level is calculated to increase by compaction from 73.0% to 100.0%, passing from a funicular state to a capillary state. On the state (3), the increment of *MC* induces the increase of ε_0 and ε_t. The material is saturated in this state. Thus, the larger amount of liquid with the increase of *MC* may have caused a dilution effect on the mixture, reducing its density and increasing the porosity. The bulk porosity is inversely related to bulk density. Therefore, as expected, the effects observed for loose and tapped bulk porosities were respectively inverse observed for loose and tapped bulk densities (Figure S3). The ε_0 and ε_t showed an exponential correlation with *MC* on states (1) and (2) and a linear correlation on the state (3). Thus, Eqs. (11) (R^2 = 0.981) and (12) (R^2 = 0.997) were proposed to describe ε_0 and ε_t in the function of *MC*.

$$\varepsilon_0 = \begin{cases} 0.15e^{0.05MC} + 0.42 & for \quad MC < 15.2\% \\ 4.44e^{-0.20MC} + 0.53 & for \quad 15.2\% \le MC < 27.6\% \\ 0.01MC + 0.23 & for \quad MC \ge 27.6\% \end{cases} \quad (11)$$

$$\varepsilon_t = \begin{cases} 0.14e^{0.05MC} + 0.31 & for \quad MC < 12.5\% \\ 4.44e^{-0.27MC} + 0.41 & for \quad 12.5\% \le MC < 21.0\% \\ 0.01MC + 0.16 & for \quad MC \ge 21.0\% \end{cases} \quad (12)$$

The influence of *MC* on the effective bulk porosity (ε_{eff}) is shown in Figure 5. This parameter represents the air-filled void volume fraction compared to the bed's total volume. As *MC* increases, the ε_{eff} increases by little at state (1), which can be expected due to the low interparticle forces previously mentioned for this state. This result also suggests that the increase of ε_0 (Figure 4) in this state is probably due to the increment of liquid-filled void volumes. Moving to substate (2a), the *MC* seems enough to increase the cohesion forces and promote the formation of air-looser beds. On the substate (2b), the increase in *MC* promoted a reduction of ε_{eff}, which can be credited to reducing those forces, allowing the particles to reorient in denser interparticle configurations. The ε_{eff} continued reducing with the increase in moisture in the state (3) up to near-zero values, in contrast to the increment of ε_0 observed for this state in Figure 4. This result suggests that liquid-filled void volumes gradually increase in detriment to reducing the air-filled ones as the material gets saturated. This parameter showed an exponential correlation with the *MC*, having two different behaviors, before and after the *MC* of 15.2%; thus, Eq. (13) (R^2 = 0.994) seems appropriate to represent this correlation.

$$\varepsilon_{eff} = \begin{cases} 3.2x10^{-4}e^{0.38MC} + 0.56 & for \quad MC < 15.2\% \\ 4.7x10^{0}e^{-0.13MC} & for \quad MC \ge 15.2\% \end{cases} \quad (13)$$

The influence of *MC* on the additional bulk porosity (ε_{add}) of drilled cuttings is shown in Figure S4. This parameter reflects the ability of the powder to release the additional amount of air trapped in the packed bed [29]. The increment of *MC* resulted in the increase of ε_{add} up to the end of the substate (2a). As previously discussed, in this substate, the increment of *MC* may induce the formation of looser uncompacted packed bed structures. Thus, more air is trapped in the packing process, which is further released in the compaction process, increasing ε_{add}. On the substate

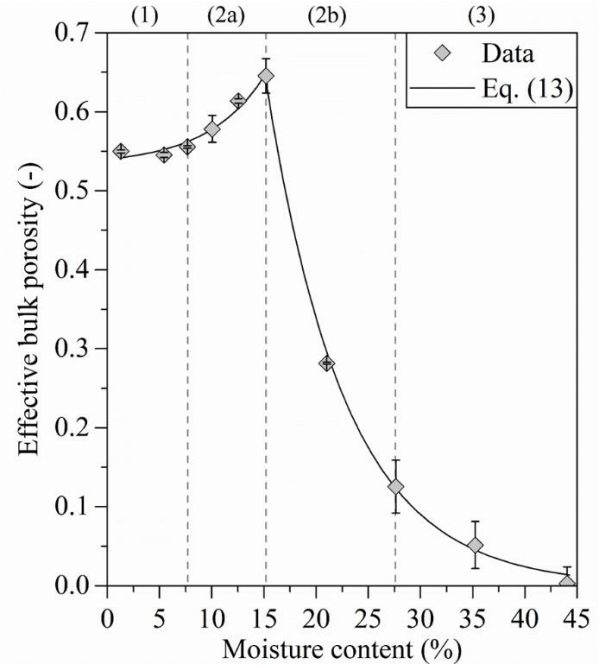

Figure 5. Effect of moisture content on the effective bulk porosity (ε_{eff}) of drilled cuttings.

(2b), the particles are believed to move more easily and form denser uncompacted bed structures, similar to the compacted ones, reducing ε_{add}. Finally, in the state (3), the voids are completely saturated, creating a liquid-solid mixture so that low amounts of air are trapped on the structure, probably in the form of bubbles, reducing the additional bulk porosity to near-zero values. As observed for ε_{eff}, ε_{add} showed an exponential correlation with the *MC*, having two different behaviors. Thus, Eq. (14) (R^2 = 0.994), similar to Eq. (13), was used to represent the relationship between ε_{add} and *MC*.

$$\varepsilon_{eff} = \begin{cases} 3.2x10^{-4}e^{0.38MC} + 0.56 & for \quad MC < 15.2\% \\ 4.7x10^{0}e^{-0.13MC} & for \quad MC \geq 15.2\% \end{cases} \qquad (14)$$

To analyze the effect of moisture on the relative facility of the particles to rearrange their positions, the granular relaxation index ($\tau_{½}$) was estimated and is shown in Figure 6. This parameter was estimated based on the compaction curves in Figure S2. On state (1), the increase in *MC* resulted in almost no change in this parameter, as expected. Nevertheless, on substate (2a), the $\tau_{½}$ increased exponentially to 15.2%. The increase of the interparticle forces with the *MC* in this state promoted the formation of steadier structures with higher bulk porosity (Figure 4, (2a)). In other words, the particles had more difficulty moving their relative positions, requiring more taps to compact the more porous packed structure. The increase of *MC* resulted in an exponential decrease of $\tau_{½}$ on the substate (2b), which indicates that the mobility of the particles was increased, probably due to the reduction of the aftermentioned interparticle forces and lubricant action of the liquid. In state (3), the voids were saturated with liquid; thus, the first taps quickly released the low amount of air trapped. Eq. (15) (R^2 = 0.978) represented the correlation between *MC* and $\tau_{½}$.

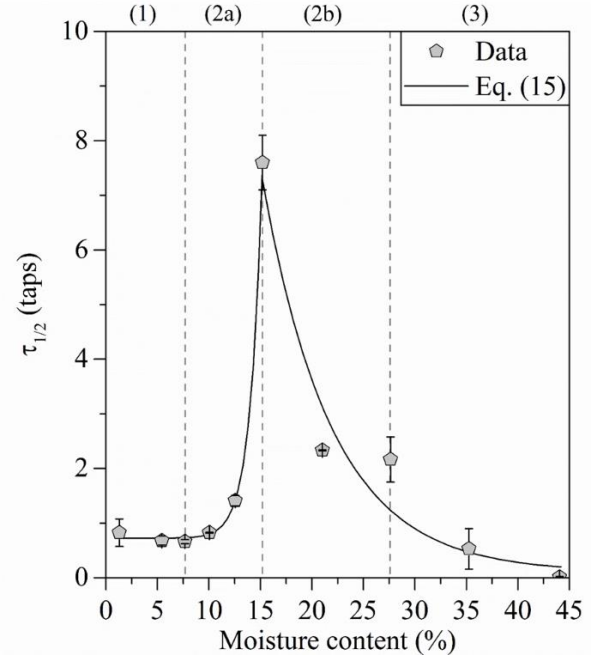

Figure 6. Effect of moisture content on the granular relaxation index ($\tau_{½}$) of drilled cuttings.

$$\tau_{1/2} = \begin{cases} 1.4x10^{-5}e^{0.86MC} + 0.72 & for \quad MC < 15.2\% \\ 6.8x10^{1}e^{-0.15MC} + 0.10 & for \quad MC \geq 15.2\% \end{cases} \qquad (15)$$

Flowability indicators

The correlation between the Hausner ratio and the angle of repose for all moisture contents analyzed is shown in Figure S5, along with the classifications of flowability [42]. A weak logarithmic tendency was perceived. Thus, Eq. (16) was fitted to the data with an R^2 of 0.996, which indicates a good adjustment to the model. It is observed that the flowability determined from *HR* corresponded to that determined using *AoR*, which highlights the coherence between the data.

$$AoR(°) = 47.377ln(HR) + 25.910 \qquad (16)$$

Figure 7 shows the Hausner ratio from drilled cuttings with different *MC*s and the flowability classifications and state limits of Figure 3. The same tendencies were also observed for *AoR*. The increment of moisture from the dry state (1) up to the end of the aggregated substate (2a) resulted in a reduction in the material's flowability from "fair" to "very poor." This phenomenon was also similarly observed by distinct authors [17,41,43] analyzing different materials and is usually attributed to increased cohesion forces. The increment of those forces may reduce the mobility

between particle-particle and particle-wall surfaces, resulting in lower flowabilities [16]. On the disaggregated (2b) and slurry (4) states, the flowability is gradually increased from "very poor" to "excellent" with the increment of moisture. This phenomenon is hypothesized to be due to the intensification of the particle surfaces' lubrication and reduction of the relative effect of cohesion forces, increasing the flowability. The Eq. (17) (R^2 = 0.999) was used to represent the correlation between MC and HR.

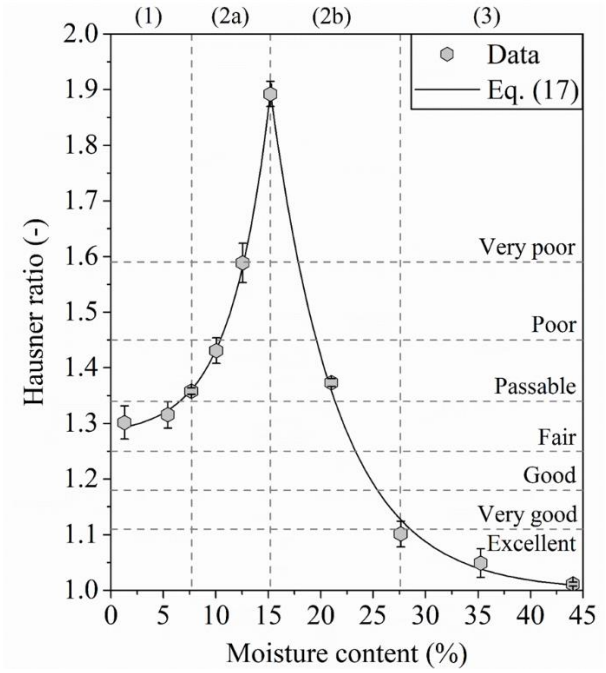

Figure 7. Effect of moisture content on Hausner ratio (HR) of drilled cuttings.

$$HR = \begin{cases} 6.8x10^{-3}e^{0.29MC} + 1.30 & for \quad MC < 15.2\% \\ 7.2x10^{0}e^{-0.13MC} + 0.95 & for \quad MC \geq 15.2\% \end{cases} \qquad (17)$$

General drilled cuttings handling behavior

Figure 8 summarizes the general effect of *MC* on the main powder handling properties studied: loose porosity (ε_0), tapped bulk porosity (ε_t) and effective porosity (ε_{eff}), additional porosity (ε_{add}), Hausner ratio (*HR*), and granular relaxation index ($\tau_{½}$). For better comparison, the data were normalized to a common scale ranging from zero to one using the following equation:

$$z_i = \frac{x_i - x_{min}}{x_{max} - x_{min}} \qquad (18)$$

where z_i is the normalized value, x_i is the non-normalized value, x_{max} is the maximum non-normalized value, and x_{min} is the minimum non-normalized value.

It is possible to notice that the increment of *MC* up to 15.2% promoted the formation of looser interparticle structures. However, these structures were steadier, showing greater difficulty flowing and releasing air/liquid. These phenomena were attributed to the increase of cohesion forces with *MC*. The continuous increment of *MC* beyond 15.2% promoted a complete change in the material behavior. The interparticle structures became denser. The material could flow and release air/liquid more easily. These phenomena were hypothesized to be due to the reduction of cohesion and friction forces (lubrication action).

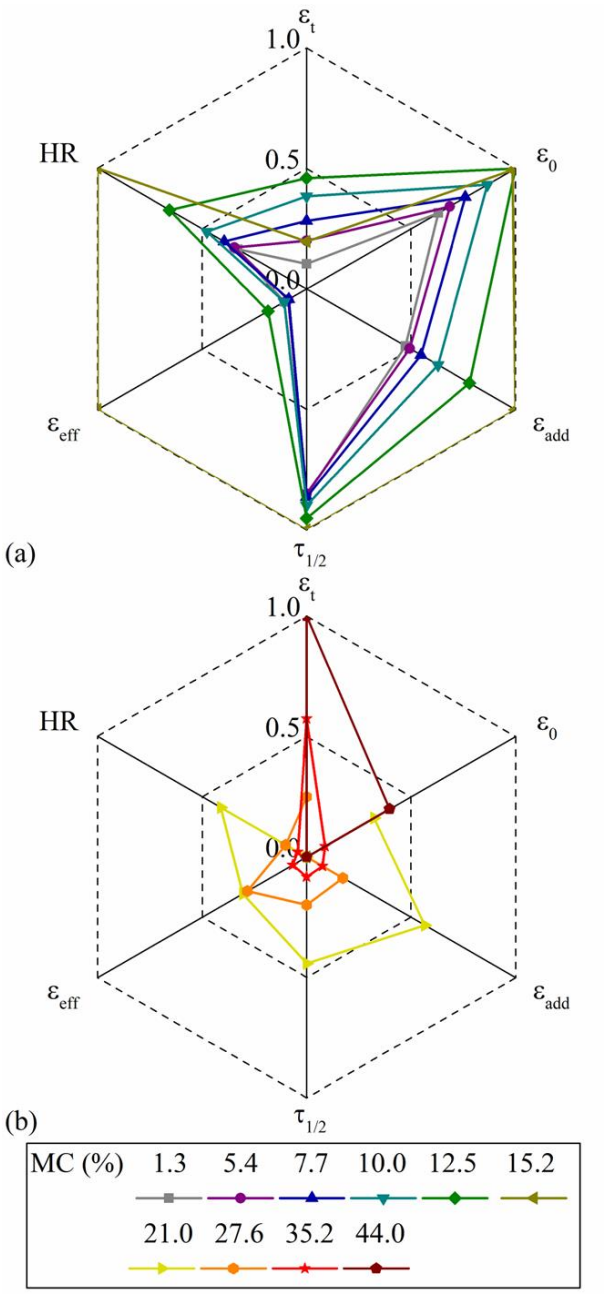

Figure 8. Summary of moisture content effects on drilled cuttings' powder handling parameters.

Generally, the drilled cuttings in the aggregated/disaggregated state (Figure 8 (10.0–21.0%)) showed the worst properties once the material showed cohesive behavior with low flowability.

Even though the addition of high *MC* in the slurry state (Figure 8 (21.0–44.0%)) promoted an apparent improvement of some properties, handling such saturated bulk material in real applications might cause unexpected problems. The material initially seems to be well flowing, but soon after a small quantity of liquid is drained off, a state is attained (state (2)) where flowability gets poor again [16]. Thus, cuttings in the dry state (Figure 8 (1.3–10.0)) seem to be the best to handle since they present more stable properties and relatively good flowability.

Bed packing and flowability properties correlations

As observed by many authors, the Hausner ratio (*HR*), Angle of repose (*AoR*), loose bulk density (ρ_0), and porosity (ε_0) can be described as functions of the mean diameter of particles (D) and Archimedes number (Ar) for several granular materials [22,43–47]. To check if there is a correlation between these parameters for drilling cuttings with different *MC*s, a multiple regression analysis was carried out by fitting Eq. (19) to the data. The analysis was also extended to the additional (ε_{add}) and effective bulk porosities (ε_{eff}) parameters.

$$y_i = ae^{bx_i} + c \tag{19}$$

where y_i is the predicted variable (*HR*, *AoR*, ρ_0, ε_0, ε_{add}, and ε_{eff}), x_i is the estimating variable (*D* or *Ar*), and *a, b,* and *c* are correlation parameters. The mean diameters of the particles/aggregates, obtained by the optical microscopy analysis (Figure 2), were used to represent D. The Ar, described by Eq. (20), is a significant parameter characterizing the interplay between the floating force and the viscous force. Specifically, it quantifies the gravitational force acting on the particles, promoting their movement and filling empty voids. Nevertheless, the same number also embodies the opposing forces, such as buoyancy and viscosity, which counteract the particles' ability to occupy these voids [22].

$$Ar = \frac{\rho_f(\rho_p - \rho_f)gD^3}{\mu^2} \tag{20}$$

where ρ_f is the fluid density, ρ_p is the particle density, *g* is the gravity acceleration, *D* is the particle mean diameter, and μ is the fluid dynamic viscosity. Some hypotheses were assumed to make this analysis possible. For MCs ≤ 21.0% (states (1) and (2)), the system was considered to be composed of particles and aggregates containing water on their surface and inner structure immersed in the air as a fluid. Therefore, ρ_p was calculated by considering the influence of the added water, and *D* was considered as the mean diameter of the particles/aggregates (Figure 2) obtained by the optical microscopy analysis for each *MC*. For MCs ≥ 21.0% (state (3)), the system was considered to be composed of particles and aggregates immersed in water as a fluid once the saturation level was at the capillary state. Thus, ρ_p was considered the actual density (ρ_r), and D was still taken as the mean diameter of the particles/aggregates.

The analysis showed that significant correlations were only obtained for ρ_0, ε_{add}, ε_{eff}, and *HR* as a function of *D* and *Ar*, as seen in Figure S6. A good correlation between *AoR* in the function of *D* and *Ar* was also observed; nevertheless, the correlations for this parameter were not shown due to the limited amount of AoR data. The results of Figures S6a and S6b showed that Eqs. (21) and (22) accurately describe (±10%) most of the values of ρ_0 in the function of *D* and *Ar*, respectively.

$$\rho_0 = 360.170e^{-4.2x10^{-2}D} + 0.777, \text{ for } 1.3\% \le MC < 21.0\% \cup 21.0\% < MC \le 44.0\% \tag{21}$$

$$\rho_0 = 1.137e^{-7.6x10^{-11}Ar} + 0.663, \text{ for } 1.3\% \le MC < 21.0\% \cup 21.0\% < MC \le 44.0\% \tag{22}$$

The ρ_0 decreases with the increase of *D* and *Ar* (Figures S6a and S6b), which was contrary to observations made by many authors [22,43–47]. However, a fundamental difference exists between the analyses conducted by these authors and the analyses presented in this paper. In those previous works, the effect of dry particles' diameters on ρ_0 is observed, resulting in a decrease in bulk density for finer particles due to van der Waals forces [45]. On the other hand, in the analyses performed in this paper, the increase in particle size is related to particle aggregation, possibly due to the increase of liquid bridge forces as the MC increases up to 15.2%. Consequently, it is expected that ρ_0 decreases with the increase of *D* as stronger liquid bridge forces form, preventing particles from rearranging into a denser configuration. For *MC* values higher than 15.2%, the values of *D* for the slurry state (3) become similar to those of the dry state (1), owing to the desegregation of the particles' clusters (Figure 2). Nevertheless, significantly higher values of ρ_0 are observed for the slurry state (3), probably because the void spaces were filled with water, increasing the bed weight. The primary influence on *Ar* is the particle size, as the *D* term is raised to the power of three in the definition of *Ar* [47]. Therefore, a similar effect of *Ar* on ρ_0 is observed. These results indicate that several complex phenomena are involved in the relationship between ρ_0, *D*, and *Ar* when the MC varies over a large range. As a result, although Eq. (21) and (22) can represent most of the data, they cannot

predict, for instance, the point of MC of 21.0%.

Figures S6c–S6f displayed that Eqs. (23–26) accurately describe (±5% or ±10%) most of the values of ε_{add} and ε_{eff} in the function of *D* and *Ar*. It is observed that ε_{add} and ε_{eff} decrease as *D* and *Ar* increase. Once again, several complex phenomena are involved, but as observed similarly for ρ_0, the results indicate that the bed becomes looser with the increase of *D* and *Ar*. It is worth noting that the use of *Ar* is preferable to *D* since the data on the slurry state can be predicted more accurately, probably because *Ar* considers the effect of the fluid properties.

$$\varepsilon_{add} = -1.051e^{-7.1x10^{-3}D} + 0.588, \text{ for } 1.3\% \le MC < 21.0\% \quad (23)$$

$$\varepsilon_{add} = -3.672e^{-5.6x10^{-12}Ar} + 3.655, \text{ for } 1.3\% \le MC < 44\% \quad (24)$$

$$\varepsilon_{eff} = -1.348e^{-1.6x10^{-2}D} + 0.617, \text{ for } 1.3\% \le MC < 15.2\% \quad (25)$$

$$\varepsilon_{eff} = -0.953e^{-1.4x10^{-10}Ar} + 0.681, \text{ for } 1.3\% \le MC < 21.0\% \cup 21.0\% < MC \le 44.0\% \quad (26)$$

Finally, Figures S6g and S6h exhibited that Eqs. (27) and (28) accurately describe (±5%) most of the values of *HR* in the function of *D* and *Ar*. However, once again, the values of *HR* in the slurry state could only be predicted in the function of *Ar*. It is also observed that *HR* increases with *D* and *Ar*, which is consistent with the hypothesis that the increase in the aggregated sizes is related to the strengthening of liquid bridge forces up to 15.2%, well-known to reduce the particle's mobility [17]. The material becomes saturated for higher MCs, leading to the disaggregation of the particle clusters and an increase in flowability.

$$HR = -3.211e^{-1.7x10^{-3}D} + 3.767, \text{ for } 1.3\% \le MC < 21.0\% \quad (27)$$

$$HR = 0.256e^{-6.0x10^{-11}Ar} + 0.745, \text{ for } 1.3\% \le MC < 44.0\% \quad (28)$$

CONCLUSION

An extensive analysis was conducted to assess the impact of moisture content on drilled cuttings, examining particle aggregation/disaggregation dynamics, packed bed properties, and flow behavior. Four characteristic states were identified according to the results: dry (1.3–7.7%), aggregated (7.7–15.2%), disaggregated (15.2–27.6%), and slurry (27.6–44.0%). The increment of moisture promoted the gradual aggregation of the particles into clusters of larger diameters in dry and aggregated states, which were disaggregated in higher moistures in the disaggregated and slurry states. Higher moisture in the dry state resulted in the creation of looser interparticle structures. Subsequent increments in moisture within the aggregated substate facilitated the emergence of air-filled void spaces, leading to even more loosely arranged structures. In the disaggregated substate, the air-filled void spaces were reduced, to the detriment of liquid-filled void spaces increase, densifying the structures. In the slurry state, the liquid-filled spaces were large enough to produce looser structures again. The flowability of the cuttings was reduced with the moisture increase from “fair” at the dry state to “very poor” at the end of the aggregated substate. By continuously increasing moisture, flowability was gradually improved on the disaggregated and slurry states up to “excellent.”

ACKNOWLEDGMENTS

The authors are grateful for financial and technical support from the Coordination for the Improvement of Higher Education Personnel (CAPES), the National Council for Scientific and Technological Development (CNPq), and Petróleo Brasileiro S.A (Petrobras®).

REFERENCES

[1] EnscoRowan, Offshore Market Recovery, EnscoRowan, Houston (2019), p. 28. https://www.valaris.com/home/default.aspx.

[2] C. Apostolidou, E. Sarris, A. Georgakopoulos, J. Pet. Sci. Eng. 208 (2022) 109758. https://doi.org/10.1016/j.petrol.2021.109758.

[3] A.K. Alkalbani, G.T. Chala, A.M. Alkalbani, Ain Shams Eng. J. 14 (2023) 102147. https://doi.org/10.1016/j.asej.2023.102147.

[4] IOGP, Drilling waste management technology review, The International Association of Oil & Gas Producer, London (2016), p. 102. https://www.iogp.org/bookstore/product/drilling-waste-management-technology-review/.

[5] S. Seaton, R.G. Morris, SPE/EPA/DOE Exploration and Production Environmental Conference, in Proceeding of SPE/EPA/DOE Exploration and Production Environmental Conference, Galveston, USA (2005) p. 157–164. https://doi.org/10.2118/94194-MS.

[6] G.A. Burnett, C. Crabb, D. Wood, K.W. Seyfert, J.M. McIntosh, US 2006/0102390A1 (2006).

[7] G.A. Burnett, C. Crabb, D. Wood, K. Seyffert, J. McIntosh, US 20070215386A1 (2007).

[8] G.A. Burnett, D. Wood, K.W. Seyffert, W.C. Herben, J.M. Mcintosh, C. Crabb, US 7195084B2 (2007).

[9] G.A. Burnett, D. Wood, K.W. Seyffert, W.C. Herben, J.M. Mcintosh, C. Crabb, EP 1766181B1 (2011).

[10] G.A. Burnett, D. Wood, K.W. Seyffert, W.C. Herben, J.M.

Mcintosh, C. Crabb, WO 2005/124096AI (2004).

[11] G.A. Burnett, C. Crabb, D. Wood, K.W. Seyffert, J. Mcintosh, EP 2165951A1 (2011).

[12] D. Mills, Pneumatic Conveying Design Guide, Elsevier, Oxford (2004) p. 650.

[13] G.E. Klinzing, F. Rizk, R. Marcus, L.S. Leung, Pneumatic Conveying of Solids: A Theoretical and Practical Approach, Springer, New York (2010) p. 600. https://doi.org/10.1080/07373939308916871.

[14] J.P. Robinson, S.W. Kingman, C.E. Snape, S.M. Bradshaw, M.S.A. Bradley, H. Shang, R. Barranco, Chem. Eng. Res. Des. 88 (2010) 146–154. https://doi.org/10.1016/j.cherd.2009.07.011.

[15] R. Pesic, T. Kaludjerovic-Radoicic, N. Boskovic-Vragolovic, Z. Arsenijevic, Z. Grbavcic, Chem. Ind. Chem. Eng. Q. 21 (2015) 419–427. https://doi.org/10.2298/CICEQ140618044P.

[16] D. Schulze, Powders and Bulk Solids, Springer, New York (2008) p. 516. 978-3-540-73768-1.

[17] A. Crouter, L. Briens, AAPS PharmSciTech 15 (2014) 65–74. https://doi.org/10.1208/s12249-013-0036-0.

[18] T.O. Althaus, E.J. Windhab, Powder Technol. 215-216 (2012) 59–65. https://doi.org/10.1016/j.powtec.2011.09.007.

[19] P. Pierrat, H.S. Caram, Powder Technol. 91 (1997) 83–93. https://doi.org/10.1016/S0032-5910(96)03179-8.

[20] H.G. Kristensen, Adv. Pharm. Sci. 7 (1995) 221–272. https://doi.org/10.1016/S0065-3136(06)80006-3.

[21] K.P. Panayiotopoulos, C.E. Mullins, J. Soil Sci. 36 (1985) 129–139. https://doi.org/10.1111/j.1365-2389.1985.tb00318.x.

[22] H. Kalman, D. Portnikov, Powder Technol. 381 (2021) 285–297. https://doi.org/10.1016/j.powtec.2020.12.019.

[23] API, Recommended Practice for Field Testing Oil-Based Drilling Fluids: API Recommended Practice 13B-2, Washington (2012), p. 67.

[24] ASTM, Standard Test Method for Sieve Analysis of Fine and Coarse Aggregates (C136-06), ASTM International, West Conshohocken (2015), p. 5. https://doi.org/10.1520/C0136_C0136M-14.

[25] P.A. Vesilind, Resour. Recover. Conserv. 5 (1980) 275–277. https://doi.org/10.1016/0304-3967(80)90007-4.

[26] ASTM, Standard test methods for determining loose and tapped bulk densities of powders using a graduated cylinder (D7481-18), American Society for Testing and Materials, (2018), p. 4. https://doi.org/10.1520/D7481-18.

[27] USP, The United States Pharmacopeia: the National Formulary, United States Pharmacopeia Convenction, Rockville (2018), p. 1136.

[28] H.O.N. Altino, G.A. Lourenço, C.H. Ataíde, Powder Technol. 391 (2021) 184–197. https://doi.org/10.1016/j.powtec.2021.06.013.

[29] K. Traina, R. Cloots, S. Bontempi, G. Lumay, N. Vandewalle, F. Boschini, Powder Technol. 235 (2013) 842–852. https://doi.org/10.1016/j.powtec.2012.11.039.

[30] ASTM, Standard Test Method for Measuring the Angle of Repose of Free-Flowing Mold Powders (C1444-00), American Society for Testing and Materials, (2000). p. 4. https://doi.org/10.1520/C1444-00.

[31] WHO. Bulk density and tapped density of powders (WHOdocument QAS/11.450), WorldHealth Organization, Dept. of Essential Medicines and Pharmaceutical Policies, (2012).

[32] K. Ishizaki, S. Komarneni, M. Nanko, Porous Materials, Springer, Boston (1998), p. 249. https://doi.org/10.1007/978-1-4615-5811-8.

[33] C. Hyun, S. Shah, S. Osisanya, SPE Annual Technical Conference and Exhibition, in Proceeding of the SPE Annual Technical Conference and Exhibition, Dallas, USA (2000), p. 905–918. https://doi.org/10.2523/63269-MS.

[34] I. Petri, M.S. Pereira, J.M. dos Santos, C.R. Duarte, C.H. Ataíde, C.M. d. Á. Panisset, J. Pet. Sci. Eng. 134 (2015) 23–29. https://doi.org/10.1016/j.petrol.2015.07.022.

[35] D. Geldart, Powder Technol. 7 (1973) 285–292. https://doi.org/10.1016/0032-5910(73)80037-3.

[36] R.J. Reeder, Carbonates: Mineralogy and Chemistry, Stony Book, New York (1983), p. 394. https://doi.org/10.1515/9781501508134.

[37] H.G. Kristensen, T. Schaefer, Drug Dev. Ind. Pharm. 13 (1987) 803–872. https://doi.org/10.3109/03639048709105217.

[38] A. Singer, Z. Barakat, S. Mohapatra, S.S. Mohapatra, Nanocarriers Drug Deliv. (2019) 395–419. https://doi.org/10.1016/b978-0-12-814033-8.00013-8.

[39] S. Golubić, J. Schneider, in Biogeochemical Cycling of Mineral-Forming, P.A. Trudinger and D.J. Swaine, Elsevier, (1979) Amsterdam, p. 122. https://doi.org/10.1016/S0166-1116(08)71056-2.

[40] P. Philippe, D. Bideau, Europhys. Lett. 60 (2002) 677–683. https://doi.org/10.1209/epl/i2002-00362-7.

[41] H. Lu, X. Guo, Y. Jin, X. Gong, Chem. Eng. Res. Des. 133 (2018) 326–334. https://doi.org/10.1016/j.cherd.2018.03.023.

[42] S. Gaisford, M. Saunders, Essentials of Pharmaceutical Preformulation, John Wiley & Sons, Chichester (2012), p. 252. https://doi.org/10.1002/9781118423226.

[43] H. Kalman, Powder Technol. 393 (2021) 582–596. https://doi.org/10.1016/j.powtec.2021.08.010.

[44] D. Geldart, E.C. Abdullah, A. Hassanpour, L.C. Nwoke, I. Wouters, Chin. Particuol. 4 (2006) 104–107. https://doi.org/10.1016/s1672-2515(07)60247-4.

[45] H. Kalman, D. Portnikov, Powder Technol. 381 (2021) 477–487. https://doi.org/10.1016/j.powtec.2020.12.014.

[46] I.M.F. Wouters, D. Geldart, Part. Part. Syst. Charact. 13 (1996) 254–259. https://doi.org/10.1002/ppsc.19960130408.

[47] H. Kalman, Powder Technol. 382 (2021) 573–593. https://doi.org/10.1016/j.powtec.2021.01.012.

HEITOR OTACÍLIO NOGUEIRA ALTINO[1]
GIOVANI AUD LOURENÇO[2]
CARLOS HENRIQUE ATAÍDE[1]
CLAUDIO ROBERTO DUARTE[1]

[1]Federal University of Uberlandia, Faculty of Chemical Engineering, Uberlândia, MG, Brazil
[2]Federal Institute of Goiás, Itumbiara, GO, Brazil

NAUČNI RAD

UTICAJ SADRŽAJA VLAGE NA SVOJSTVA I PROTOČNOST PAKOVANOG SLOJA OD OTPADAKA BUŠENJA

Za projektovanje i upravljanje različitom opremom sistema za kontrolu čvrstih materija u platformama za bušenje na moru, važno je utvrditi kako sadržaj vlage utiče na karakteristike otpadaka od bušenja koja utiču na formiranje pakovanih slojeva i strujanje preko čvrstih površina. Ovaj rad pruža sveobuhvatnu analizu o tome kako sadržaj vlage, prvenstveno sastavljen od vode i koji predstavlja mulj na bazi vode (VBM), utiče na svojstva i protočnost pakovaog sloja otpadaka. Analizirana je dinamika agregacije/deagregacije čestica, nasipne mase i poroznosti rastresitog i zbijenog sloja, dinamika zbijanja pakovanih slojeva, Hausnerov koeficijent i ugao nagiba otpadaka sa deset različitih sadržaja vlage (1,4–44,0 tež%). Uočeno je da povećanje sadržaja vlage do 15,2% podstiče formiranje labavije interčestične strukture. Međutim, ove strukture su bile stabilnije, pokazujući veće teškoće pri proticanju i oslobađanju vazduha/tečnosti. Kontinualno povećanje sadržaja vlage preko 15,2% je doprinelo potpunoj promeni ponašanja materijala. Međučestične strukture postale su gušće. Materijal je mogao lakše da teče i oslobađa vazduh/tečnost. Pored toga, bilo je moguće uspostaviti klasifikaciju različitog ponašanja otpadaka prema sadržaju vlage. Predloženi su prediktivni modeli za opisivanje uticaja sadržaja vlage na svojstva i protočnost pakovanog sloja od otpadaka bušenja..

Ključne reči: agregacija čestica, dezagregacija čestica, pakovani sloj, protočnost, zbijanje.